Biosensors and Bioelectronics ■ (■■■■) ■■■–■■■

Contents lists available at ScienceDirect

Biosensors and Bioelectronics

journal homepage: www.elsevier.com/locate/bios

Antithyroid drug detection using an enzyme cascade blocking in a nanoparticle-based lab-on-a-chip system

Sevinc Kurbanoglu [a,b], Carmen C. Mayorga-Martinez [a], Mariana Medina-Sánchez [a], Lourdes Rivas [a], Sibel A. Ozkan [b], Arben Merkoçi [a,c,*]

[a] Nanobioelectronics & Biosensors Group, ICN2- Institut Catala de Nanociencia i Nanotecnologia, Campus UAB, 08193 Bellaterra, Barcelona, Spain
[b] Ankara University, Faculty of Pharmacy, Department of Analytical Chemistry, 06100 Tandogan, Ankara, Turkey
[c] ICREA, Barcelona, Catalonia, Spain

ARTICLE INFO

Article history:
Received 6 June 2014
Received in revised form
4 October 2014
Accepted 7 October 2014

Keywords:
Methimazole detection
Enzyme inhibition
Magnetic nanoparticles
Iridium oxide nanoparticles
Lab-on-a-chip system

ABSTRACT

A methimazole (MT) biosensor based on a nanocomposite of magnetic nanoparticles (MNPs) functionalized with iridium oxide nanoparticles (IrOx NPs) and tyrosinase (Tyr) immobilized onto screen printed electrode (SPE) by using a permanent magnet is presented. This system is evaluated in batch mode via chelating copper at the active site of tyrosinase and in flow mode by thioquinone formation. The MT detection in flow mode is achieved using a hybrid polydimethylsiloxane/polyester amperometric lab-on-a-chip (LOC) microsystem with an integrated SPE. Both systems are very sensitive with low limit of detection (LOD): 0.006 μM and 0.004 μM for batch and flow modes, respectively. Nevertheless, the flow mode has advantages such as its reusability, automation, low sample volume (6 μL), and fast response (20 s). Optimization and validation parameters such as enzyme–substrate amount, flow rate, inhibition conditions, repeatability and reproducibility of the biosensor have been performed. The proposed methods have been applied in MT detection in spiked human serum and pharmaceutical dosage forms.

1. Introduction

Methimazole (MT, 1-methyl-2-mercaptoimidazole) is an antithyroid agent which is widely used in medicine for treatment of hyperthyroidism. It is a well-known classical non-competitive inhibitor for all isoforms of cytochrome P450 and flavin-containing monooxygenases (Chung et al., 2000; Hashizume et al., 1977). MT is absorbed by the gastrointestinal tract and concentrates in the thyroid gland. It inhibits the production of thyroid hormones due to its action that decreases the iodide incorporation into tyrosine (Kasraee, 2002; Siénko et al., 2006). It is one of the orally active drugs used in the therapy of hyperthyroidism (Edward, 1992; Gheibi et al., 2005). However, the MT detection is important in clinical chemistry and pharmaceutical formulations, because this drug also causes side effects such as nephritis, liver cirosis, irritation of the skin, allergies and pharyngitis with fever as well as impaired taste, olfactory and auditory disorder (Economou et al., 2004; Aslanoglu and Peker, 2003; Yazhen, 2011).

In the literature, different analytical procedures have been developed for the determination of methimazole such as gas chromatography–mass spectrometry (Zhang et al., 2005), high-performance liquid chromatography–mass spectrometry (DeWasch et al., 2001) and flow-injection with ultraviolet detection (Hollosi et al., 2004). On the other hand, enzymatic biosensors are used for different analytes detection based in inhibition systems. Thereby, MT inhibits the Tyr-based biosensors system in two ways. In the first one, when MT is added to the solution, MT immediately reacts with *o*-quinones and forms thioquinone (Raoofz et al., 2012; Stonea et al., 2003). In the second way, MT can inhibit Tyr by chelating copper at the active site of Tyr. As tyrosinase loses copper, the conformation of the enzyme changes and irreversible inhibition occurs (Lerch, 1981; Solomon et al., 1996).

Nanostructured materials possess unique optical, electronic and magnetic properties depending on their core materials and they have large surface-to-volume ratio that favors miniaturization (Marn and Merkoçi, 2012; Pérez-López and Merkoçi, 2011). In the last few years, nanostructured materials such as magnetic nanoparticles (MNPs) have been reported in a wide range of applications that include the immobilization of cells, enzymes (Betancor et al., 2005), proteins and nucleic acids (Grieshaber et al., 2008, Li et al., 2011; Yeh et al., 2010). Among various nanostructured materials, iridium oxide nanoparticles (IrOx NPs)

* Corresponding author at: Nanobioelectronics & Biosensors Group, ICN2- Institut Catala de Nanociencia i Nanotecnologia, Campus UAB, 08193 Bellaterra, Barcelona, Spain.
E-mail address: arben.merkoci@icn.cat (A. Merkoçi).

http://dx.doi.org/10.1016/j.bios.2014.10.014
0956-5663/

attract attention in the design of novel electrochemical sensors for their stability and catalytic properties (Tolosa et al., 2013; Mayorga-Martinez et al., 2008, 2014b).

In recent years, lab-on-a-chip (LOC) platforms have been approved as new materials for electrochemical sensing. They have numerous advantages in terms of response speed, low cost, portability, small sample and reagent consumption, and low energy requirements (Pumera et al., 2006). Designing a LOC device is related to a very important factor to achieve an ultimate goal: sensing small amount of sample with a low limit of detection. Generally, polymer or silicon based chip materials are chosen as substrates in LOC design. Polymer-based substrates are more common and preferentially chosen compared to silicon-based substrates due to their easy fabrication without any micromachining technology. Fabrication of microfluidic systems in elastomeric poly (dimethylsiloxane) (PDMS) is simpler, easy to fabricate and biocompatible compared to other polymers (Duffy et al., 1998; Medina-Sánchez et al., 2012b; Ren et al., 2013, 2014; Mayorga-Martinez et al., 2013b).

In this work, a sensible MT biosensing system based on inhibition of Tyr through chelating copper at the active site and thioquinone formation using a biocomposite of MNPs, IrOx NPs and Tyr is evaluated. The optimization of the biocomposite formation in relation to enzyme, IrOx NPs and MNPs′ amounts and the incubation time has first been performed, and this was then followed by the analytical characterization of the catechol response in both batch and LOC formats. This system is performed in batch and LOC systems by Tyr inhibition and thioquinone formation, respectively. The fully validated inhibition methods have been applied to spiked human serum and pharmaceutical dosage forms containing MT. Both systems present high analytical performance in terms of linear range and limit of detection. Nevertheless, the LOC mode represents a more promising system for automated and rapid response applications.

2. Materials and methods

2.1. Reagents

Tyrosinase from mushroom ($\geq$1000 unit/mg), catechol and methimazole were purchased from Sigma-Aldrich (St. Louis, MO). For the synthesis of iridium oxide nanoparticles, potassium hexachloroiridate-(IV), sodium hydrogencitrate were purchased from Sigma-Aldrich (St. Louis, MO). Milli-Q water was obtained from purification system and all solutions were prepared with ultrapure water from a Millipore-Milli-Q system. For the preparation of LOC system, Kapton Polyimide Adhesive Tape, (3 in. Core, 2 mm thick, 36 Yd length, 3/4 in. width, 127 μm of thickness) was obtained from Katco Ltd., United Kingdom. Poly (dimethylsiloxane) and 3-aminopropyltriethoxylane were purchased from Sigma Aldrich (St. Louis, MO). NH_2 functionalized magnetic nanoparticles were purchased from Chemicell GmbH, Germany. Human serum from human male AB plasma was purchased from Sigma-Aldrich (St. Louis, MO).

2.2. Morphological characterization

Scanning electron microscopy (SEM) images were acquired using a Field Emission-Scanning Electron Microscopy (Merlin, Carl Zeiss).

2.3. Synthesis of iridium oxide nanoparticles

In order to synthesize iridium oxide nanoparticles, 2.6×10^{-5} M potassium hexachloroiridate-(IV) solution was mixed with 1.6×10^{-2} M sodium hydrogencitrate solution. The pH of the red brown solution was adjusted to pH 7.5 with 0.25 M NaOH. After that, it was refluxed in an oil bath with constant stirring for 30 min. As the mixture cooled to room temperature, the pH was again adjusted to 7.5 with a reflux for 30 min. This procedure was repeated until pH reached a constant value of 7.5. As a final point, the solution was refluxed again for 2 h under oxygen bubbling and a deep blue solution of IrOx NPs was obtained (Kuwabara et al., 2008). The solution was stocked in a glass-stopper flask at 4 °C when not in use.

2.4. SPE and lab-on-a-chip systems fabrication

As the electrochemical detector, screen printed carbon electrodes (SPEs) consisted of a set of three electrodes: carbon working electrode with a diameter of 3 mm, Ag/AgCl pseudo reference electrode (with a potential of 10 mV with respect to a commercial Ag/AgCl electrode) and carbon counter electrode with an approximate thickness of 4 μm were used. Screen printing electrodes were fabricated by sequential deposition of a graphite ink (Electrodag 423SS), Ag/AgCl ink and insulating ink on a polyester substrate using a screen-printing machine (DEK 248, DEK International, Switzerland). Firstly, the graphite layer was printed onto the polyester sheet and cured at 120 °C for 40 min. The reference electrode was obtained by printing a second layer Ag/AgCl ink which was cured under the same conditions. An insulator ink was covered and cured again at 120 °C for 40 min. All the inks were purchased from Acheson Industries, Germany.

Lab-on-a-chip system was fabricated by rapid and very cheap prototyping using PDMS technology. Briefly, a glass slide was used as a substrate, on which a very strong adhesive kapton tape was attached with the shape of the desired channel geometry (Renaudot et al., 2013; Kortmann et al., 2009). Then, the PDMS channel and the polyester substrate were assembled using a previously reported protocol (Xia and Whitesides, 1998; Tang and Lee, 2010). The PC substrate was treated by air–plasma for 1 min and then immersed into a 2% (v/v) of 3-aminopropyltriethoxylane solution in water for 1 h. The surface of the PDMS channel was also activated for 1 min by plasma, and put into contact with the polyester sheet to achieve irreversible bonding (Medina-Sánchez et al., 2012a, 2012b). Once the counter and reference electrode were printed, a hole was opened in order to attach a disposable working electrode. Finally, the disposable working electrode was attached behind the polyester substrate, which was aligned with the hole previously done, using a double sided adhesive tape (Li et al., 2011). In order to complete the fabrication of the electrochemical magneto microfluidic sensor, a magnet was attached using a double sided adhesive tape (Fig. 1E). For the electrochemical measurements, a homemade connector was used for coupling with Autolab. The Harward apparatus Pump 11 elite pumps and Hamilton syringe were used to achieve sample injection in lab-on-a-chip system.

2.5. Preparation of IrOx NPs/Tyr/MNPs nanocomposite

IrOx NPs suspension (250 μL) was shaken with 20 μL of Tyr solution of 19.61 U during 12 h at 4 °C. After that, 50 μL of NH_2 functionalized MNPs were added to the mixture, and shaken at 4 °C for 12 h. 8 μL of the resulting nanocomposite was dropped onto the working electrode of SPE and it was pre-concentrated by using magnet under the working electrode of SPE.

Please cite this article as: Kurbanoglu, S., et al., Biosensors and Bioelectronics (2014), http://dx.doi.org/10.1016/j.bios.2014.10.014

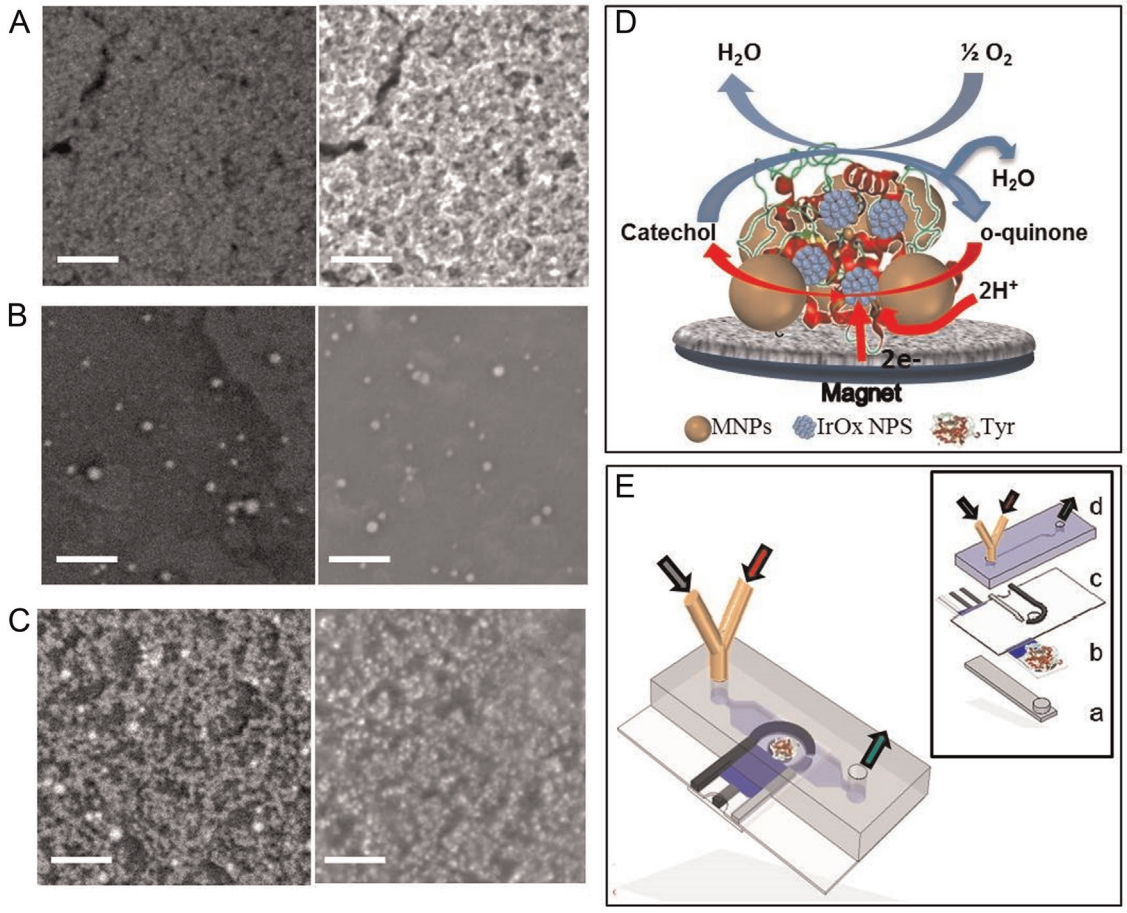

Fig. 1. SEM images of MNPs and Tyr (A), IrOx and Tyr (B) and IrOx NPs–Tyr-MNPs nanocomposite (C). Scale bars of SEM images are 100 nm. The SEM images were obtained using backscatter electrons (BE) mode (left column) and secondary electron (SE) mode (right column). (D) Schematic representation of the proposed detection system displaying tyrosinase (Tyr) and the reaction involved in the catechol detection. (E) Lab-on-a-chip design inset: (a) magnet, (b) interchangeable SPE, (c) PE substrate (RE and CE), and (d) PDMS channel.

2.6. MT detection from its pharmaceutical dosage forms and spiked human serum

For detecting MT from pharmaceutical dosage forms, 10 Tirodril® film-coated tablets containing 5 mg MT were accurately weighed, crushed and finely powdered. A quantity of the powder equivalent to one tablet content was accurately weighted and transferred into a 50 mL volumetric flask which was then diluted with phosphate buffer (PB) and sonicated about 10 min. This solution was filtered and the filtrate was used to prepare solutions by taking suitable aliquots of the clear filtrate. After diluting them with PBs, a final solution was obtained. The MT detection from human serum (human male AB plasma) was achieved by recovery tests after addition of known amounts of pure drug to the human serum plasma and dilution with PB. Applicability of the proposed method was confirmed by utilizing recovery studies both in pharmaceutical analysis and human serum analyzes.

2.7. Electrochemical measurements

Electrochemical experiments were performed using an electrochemical analyzer Autolab 20 (Eco-Chemie, The Netherlands) which was connected to a personal computer using a software package GPS 4.9 (General Purpose Electrochemical System). Chrono-amperometric measurements were conducted at −100 mV. Cyclic voltammograms were recovered the potential range of −800–+800 mV with scan rate of 50 mV/s. All electrochemical experiments were carried out at room temperature using 0.1 M phosphate buffer with 0.1 M KCl.

3. Results and discussion

3.1. Morphological studies

The Scanning Electron Microscope (SEM) images were captured to observe the morphology of each component of the nanocomposite. Fig. 1A, B and C show the SEM images of MNPs and Tyr, the bioconjugate formed between the IrOx NPs and tyrosinase (Tyr), and the product of the IrOx NPs–Tyr bioconjugate interaction with MNPs, respectively. The images were obtained using backscatter electrons (BE) mode (left column) and secondary electron (SE) mode (right column). In Fig. 1B and C, it is possible to observe the IrOx NPs as bright dots using BE mode. An enhancement of the contrast between IrOx NPs with other components of different chemical composition is well appreciated.

3.2. Optimization of the catechol detection

The best biosensing response toward catechol detection was optimized using different strategies during the preparation of IrOx NPs/Tyr/MNPs biocomposite. Different parameters such as shaking (incubation) time (6 h and 12 h) of the mixture of Tyr with IrOx NPs (Fig. S1A), IrOx NPs amount (250, 125, 375 μL) (Fig. S1B) and Tyr amount (19.61 U, 4.9 U, 9.81 U) (Fig. S1C) were evaluated. The

best response was found when 250 µL IrOx NPs and 19.61 U Tyr were mixed for 12 h. Table S1 shows analytical performances during the optimization tests using various conditions.

Cyclic voltammograms (Fig. S2) of SPE/MNPs (curve a), SPE/MNPs/Tyr (curve b) and SPE/MNPs/Tyr/IrOx NPs (curve c) in the presence of 1 mM catechol were recorded. In all the cases the CV shows one anodic and one cathodic peak which correspond to the transformation of catechol to *o*-quinone and vice versa within a two-electron process in 0.1 M phosphate buffer at pH 6.5 with 0.1 M KCl (Papouchado et al., 1972, 1968; Rayn et al., 1980). *O*-quinone is the product of catechol oxidation through Try catecholase activity (see Reaction (1)). Tyrosinase (Tyr, EC 1.14.18.1) is a bifunctional copper-containing enzyme that has both cresolase and catecholase activities. Tyr catalyzes the o-hydroxylation of monophenols to the corresponding catechols (called as cresolase activity), and the oxidation of catechols to the corresponding *o*-quinone (called as catecholase activity) (Mayorga-Martinez et al., 2013a, 2013b, 2014a, 2014b; Mason, 1957). The electrocatalytic activity of the MNP/Tyr/IrOx NPs platform for catechol detection can be observed through electro-chemically reduced o-quinone to catechol at low applied negative potentials (see Reaction (2)). The schematic representation of the proposed mechanism for catechol detection using this system is shown in Fig. 1D.

$$\text{Catechol} \overset{\text{Tyrosinase}}{\underset{O_2}{\Longrightarrow}} o\text{–quinone} + H_2O \quad (1)$$

$$o\text{–quinone} + 2H^+ + 2e^- \underset{-E\ mV}{\Longrightarrow} \text{catechol} \quad (2)$$

The designed MNPs/IrOx NPs/Tyr biosensor shows higher response with $\Delta Ep = +364$ mV (Fig. S2A, curve c) compared to SPE/MNPs/Tyr biosensor (curve b) and SPE/MNPs (curve a) with ΔEp of +591 and +652 mV, respectively. The presence of IrOx NPs decreases the ΔEp value and therefore, the electron transfer rate increases. This phenomena is maybe due to the fact that IrOx NPs is a metallic oxide known for its high conductivity that corresponds to the high oxidation state (4+) of iridium (Mayorga-Martinez et al., 2014b, 2008). On the other hand, the use of magnetic nanoparticles for immobilization of Tyrosinase and IrOx NPs represented an interesting pre-concentration platform, where the uses of other materials like polymers or cross-linked agent are not necessary.

Fig. S2B shows the chronoamperometric responses of SPE modified with MNPs, MNPs/Tyr and MNPs/ Tyr/ IrOx NPs for successive additions of 0.2 µM catechol while applying a −100 mV potential, this potential is previously optimized (see Fig. S1D). As observed, the catechol response increases when IrOx NPs present in the detection system shows its role in the current sensitivity improvement.

The chronoamperometric response of the MNPs/Tyr/IrOxNPs biosensor to successive additions of catechol at different concentrations (Fig. 2A) was further evaluated. As shown in Fig. 2B a linear biosensor response for catechol with $r = 0.99$ within a wide range (from 23.5 to 433.50 µM) was observed. Moreover, within 10 s after each addition of catechol, sensitive bioelectrocatalytic response reaches about 95% of the steady-state current. Limit of detection (LOD) and limit of quantitation (LOQ) values of the developed biosensor were calculated according to the 3 s/m and 10 s/m criteria, respectively, where '*s*' is the standard deviation of the peak currents of low concentration of the analyte and '*m*' is the slope of the related calibration graph (Ermer, 2005; Ozkan, 2012). The biosensor shows LOD and LOQ values as 0.043 µM and 0.13 µM, respectively for catechol.

On the other hand, the catechol detection in LOC was optimized using 20 µL injection volume and 50 µL min^{-1} flow rate (these conditions were chosen from various optimization experiments). Two pump systems were used being one responsible for buffer or

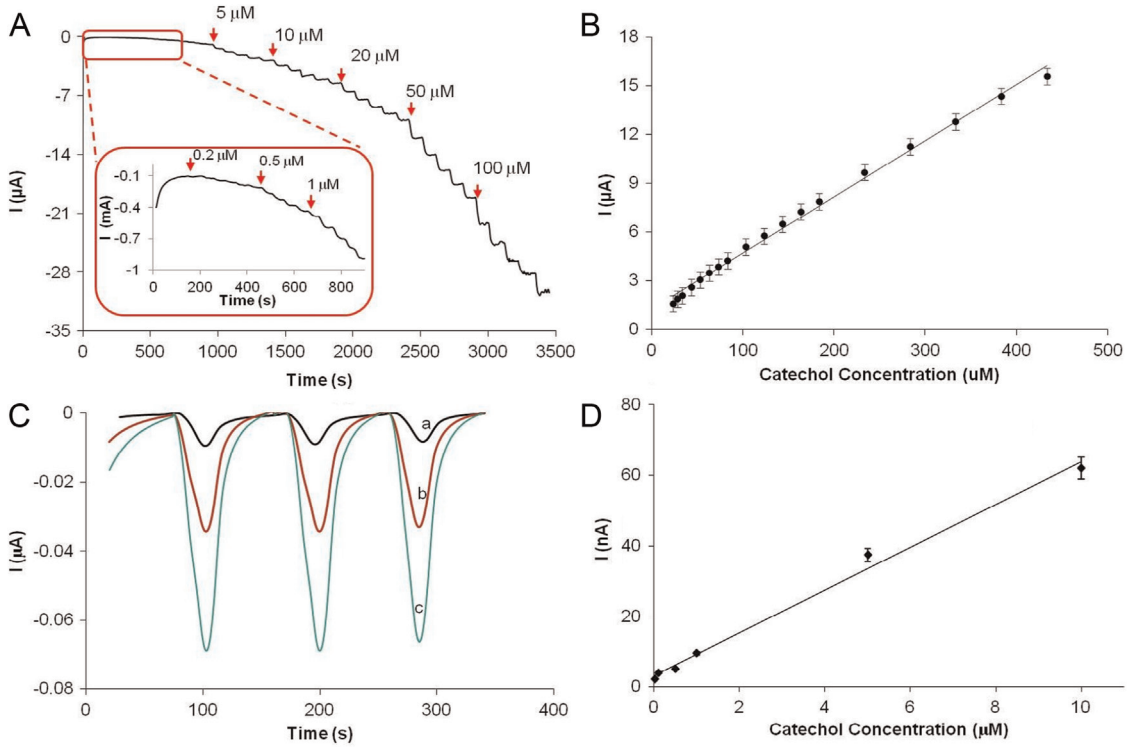

Fig. 2. Typical current–time response curves for the successive additions of catechol to optimized SPE/MNPs/IrOxNPs/Tyr biosensor (A), biosensor calibration given as current versus catechol concentration using optimized SPE/MNPs/IrOxNPs/Tyr biosensor (B), increasing concentrations of catechol ($a = 0.1$ µM, $b = 0.25$ µM, $c = 0.5$ µM) responses using designed microchip (C), and biosensor calibration given as current versus catechol concentration using designed microchip (D).

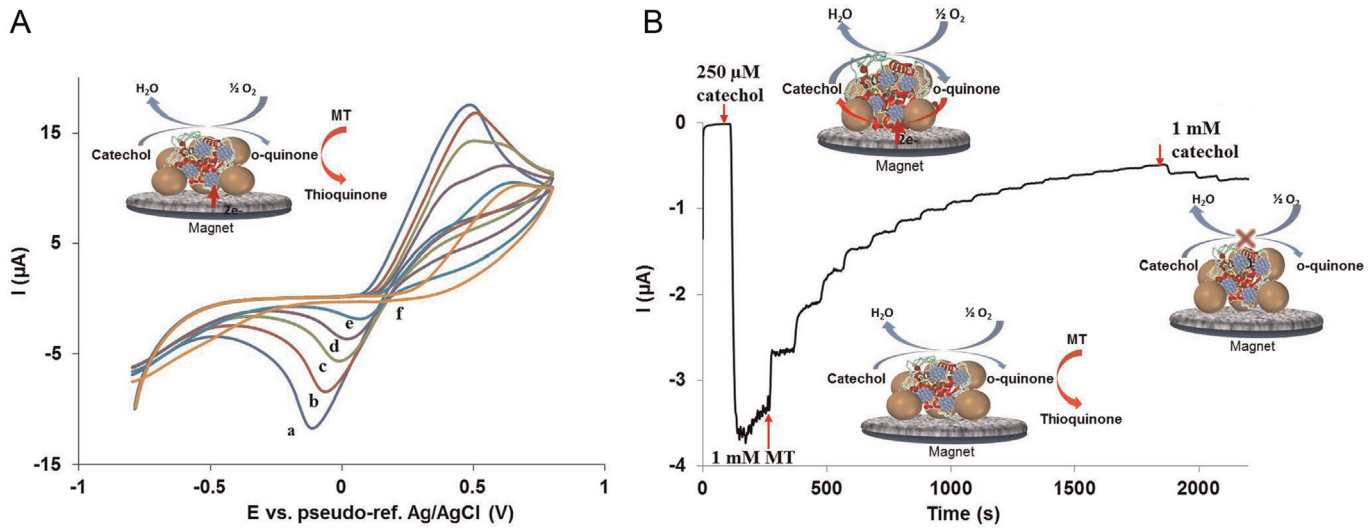

Fig. 3. Methimazole detection (A) conjugating with *o*-quinones: cyclic voltammograms of 1 mM catechol with different concentrations of methimazole (a) 1 mM catechol, (b) mixture of 1 mM catechol and 0.2 mM MT, (c) mixture of 1 mM catechol and 0.4 mM MT, (d) mixture of 1 mM catechol and 0.6 mM MT, (e) mixture of 1 mM catechol and 0.8 mM MT, and (f) 1 mM MT); (B) chrono-amperometric measurements 250 μM catechol, continuous addition of 1 mM methimazole and 1 mM catechol.

drug flow, and the other one for the injection of the catechol. Fig. 2C shows that when the catechol concentrations increase, higher current response is observed using designed microchip.

The reliable catechol responses were obtained (Fig. 2C) in a linearity range between 0.01 μM and 10 μM with $r=0.99$. LOD and LOQ values are also calculated as 0.003 and 0.009 μM, respectively, for catechol detection (Fig. 2D). Within-day repeatability measurements are also shown as the results of triplicate sets indicated by error bars in Fig. 2D. Relative standard deviation (RSD) values for both batch and LOC are lower than 15% for between day repeatability and lower than 10% for within-day repeatability.

3.3. Methimazole detection

To investigate the MT detection through inhibition of Tyr, the designed biosensor based on nanocomposite of magnetic nanoparticles functionalized with iridium oxide nanoparticles and tyrosinase immobilized onto screen printed electrode by using a permanent magnet is further used. The cyclic voltammograms of 1 mM catechol in presence of MT with different concentrations are registered (Fig. 3A). These results show that decrease in the reduction current goes proportionally with the increase of MT concentration. This phenomenon is due to the fact that MT

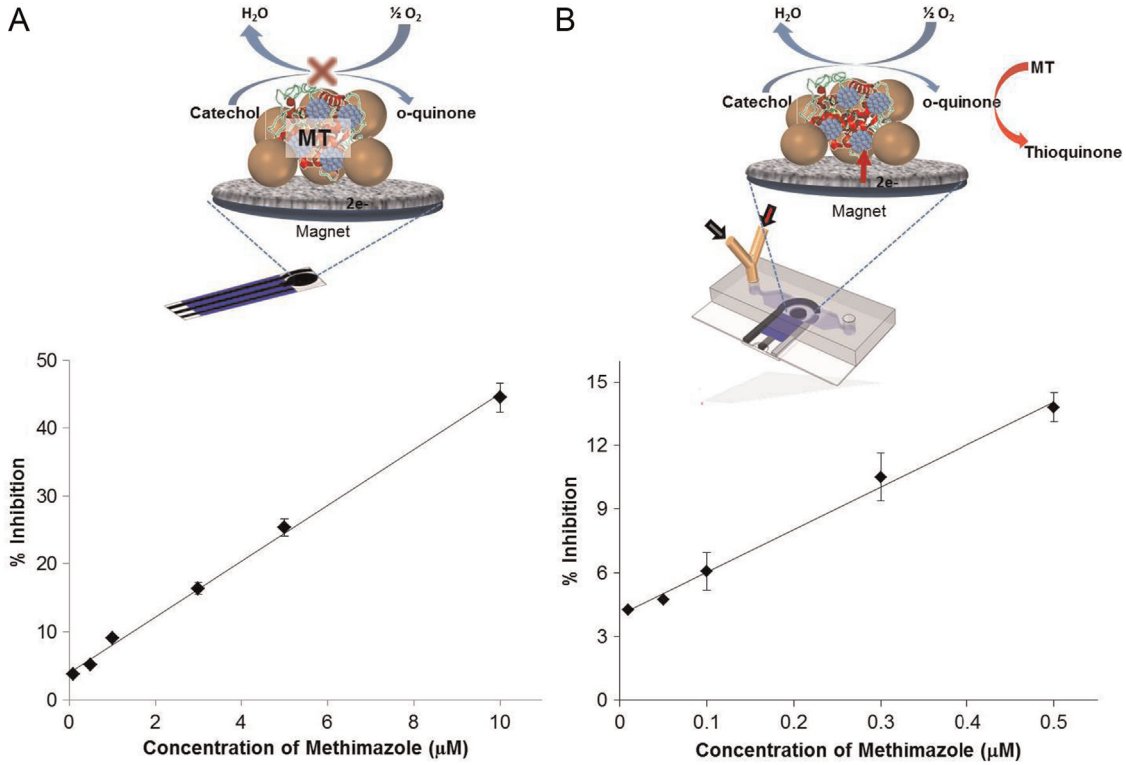

Fig. 4. Calibration graph for methimazole detection strategies (A) Tyr inhibition in batch and (B) thioquinone formation in LOC with respective mechanisms.

immediately reacts with *o*-quinones and forms thioquinone (see Reaction (3)) (Raoofz et al., 2012; Stonea et al., 2003). Therefore, cycling between the *o*-quinone to catechol cannot occur. The schematic representation of the proposed mechanism is presented as inset of Fig. 3A.

$$\text{Catechol} \overset{\text{Tyrosinase}}{\underset{O_2}{\Longrightarrow}} o\text{–quinone} + H_2O \quad (1')$$

$$o\text{–quinone} + \text{methimazole} \rightarrow \text{thioquinone} \quad (3)$$

Chronoamperometric measurements also show the effect of methimazole onto the Tyr-based system (Fig. 3B). As high concentration of catechol (250 μM) is added to the Tyr-based system (see inset of mechanism for catechol detection) a significant change in the current (ca. 3.8 μA) is observed. When 1 mM MT is added to the same system, a decrease in the signal corresponding to the thioquinone formation is observed (see inset of mechanism for thioquinone formation). Further additions of MT (up to 16 mM) are done to see the decrease in the catechol response with every addition due to thioquinone formation. After that, 1 mM catechol is added to the same system. The observed decrease in catechol response is related to the fact that MT inhibits Tyr by binding the copper at the active site of Tyr. An inset in Fig. 3B shows the schematic representation of mechanism for Tyr inhibition.

Methimazole detection by chelating copper at the active site of Tyr is performed through batch measurement. Fig. 4A shows the change of the 'percentage of inhibition' (I %) versus MT concentration. I% is calculated as

$$I\% = \left(\left(I_{ss} - I_p\right)/I_{ss}\right)100 \quad (4)$$

where I_{ss} current corresponds to the enzyme activity of the biosensor when the inhibitor (MT) is not present. Lower steady state-currents (I_p) refer to the catechol response after inhibition with MT (from 0.1 to 10 μM). For optimizing the incubation time, biosensing response for 10 μM catechol is recorded. The same biosensor is incubated in 5 μM MT for different incubation times (1, 5, 10 and 30 min). The optimum incubation time for 23.17 ± 2.67% inhibition is found at 5 min as shown in Fig. S3A. Moreover, different concentrations of catechol (1, 5 and 10 μM) are also tested, and the best inhibition response (25.39 ± 1.06%) is found to be achieved for a 10 μM substrate solution (Fig. S3B). Under optimized inhibition conditions, the purposed biosensor provides linearity range for MT concentration from 0.1 to 10 μM with a correlation coefficient of 0.999 and LOD, LOQ values are 0.006 and 0.017 μM, respectively. As the MT irreversibly inhibits the enzyme, a new biosensor was used for each point of the calibration after being exposed to the MT solution. The results indicated by error bars reveal the within-day repeatability (Fig. 4A). RSD values for both within-day repeatability and between days repeatability are lower than 15%.

MT detection by thioquinone formation is performed in LOC mode. The measurement is performed in continuous flux of MT (from 0.1 to 10 μM) at 50 μL min^{-1} of flow rate, followed by injections of 20 μL of 1μM catechol at 50 μL min^{-1} of flow rate.

From the plots of the biosensor inhibition percentage as a function of MT concentration, a linear range between 0.01 μM and 0.5 μM MT with r=0.99 was obtained. LOD and LOQ values were also calculated as 0.003 and 0.010 μM MT, respectively, as shown in Fig. 4B and Table 1. RSD values for both in-day repeatability and between days repeatability are lower than 15%. All the analytical parameters obtained for both inhibition methods in LOC and batch systems are summarized in Table 1. When LOC and batch methods are compared, it can be concluded that although batch method had wider linearity range, LOC method is more sensitive with respect to LOD and LOQ values. LOD value is 1.5 and LOQ value of LOC system is 2 times lower than batch. Moreover, LOC-based method showed better RSD% values for within-day (4.33%) and between-day precisions (5.56%) as shown in Table 1.

Table 1
Regression data for both detection strategies of methimazole.

	Batch	LOC
Linearity range (μM)	0.1–10	0.01–0.5
Slope (μA M^{-1})	4.10	20.00
Intercept (μA)	3.96	4.03
S.E. of slope	1.07×10^{-1}	8.69×10^{-1}
S.E. of intercept	5.08×10^{-1}	2.31×10^{-1}
Correlation coefficient	0.99	0.99
Limit of Detection (μM)	0.006	0.003
Limit of Quantification (μM)	0.02	0.01
Within-day precision[a] (RSD %)	6.61	4.33
Between-day precision[a] (RSD %)	6.64	5.56
Reproducibility of the electrode (RSD %)[a]	4.16	4.33

[a] Each value is the mean of five experiments.

3.4. Application to real samples

To further demonstrate the applicability of the proposed methods in pharmaceutical dosage form analysis, a commercial medicinal sample containing methimazole, Tirodril® was analyzed. To determine whether excipients in the dosage form interfere with the analysis, the accuracy of the proposed methods were evaluated by recovery tests after addition of known amounts of pure drug to the pre-analyzed formulations of MT.

Moreover, MT detection from spiked human serum plasma was achieved by recovery tests. The results show the validity of the proposed techniques for the quantitative determination of MT as shown in Table 2.

Interference studies were also performed following continuous addition of 25 μM ascorbic acid, uric acid and paracetamol at a 25 μM catechol solution. From chronoamperometric measurements shown in Fig. S4, it is clear that the system is not affected by the studied species as possible interferents.

4. Conclusions

A novel biosensor based on the use of a biocomposite made of MNPs, IrOx NPs and tyrosinase for methimazole detection is developed. The MT detection is based on inhibition of Tyr-based system through thioquinone formation and chelating copper at the active site of tyrosinase. The MT detection by chelating copper at the active site of tyrosinase is performed in batch measurement while the detection of MT by conjugation with o-quinone to form

Table 2
Detection of MT from spiked human serum and pharmaceutical dosage form Tirodril®.

	PHARMACEUTICAL Tirodril®		HUMAN SERUM	
	Batch	LOC	Batch	LOC
Label Claimed (mg)	5.00	5.00	–	–
Found (mg)	5.35	4.90	–	–
%RSD	5.44	3.37	–	–
%Bias	−7.00	2.00	–	–
Added (μM)	10.00	0.50	5.00	0.50
Found (μM)	10.71	0.50	5.22	0.52
Recovery (%)	107.13	100.04	104.39	103.63
%RSD	6.89	3.74	3.43	4.29
%Bias	−7.13	−0.04	−4.40	−4.00

thioquinone is performed in a LOC system. Due to the high conductivity of the IrOx NPs, the proposed biosensor displays improvements of the analytical performance in terms of linear ranges for catechol between 3 and 433 μM. For MT detection in LOC system, linear range between 0.01 μM and 0.5 μM MT concentration with LOD and LOQ values of 0.003 μM and 0.010 μM MT were obtained, respectively. The developed biosensor in batch provides linearity range for MT concentration from 0.1 to 10 μM with a correlation coefficient of 0.999 and LOD, LOQ values are 0.006 and 0.017 μM, respectively. The characterization and optimization of the biosensor in terms of enzyme, substrate, IrOx NPs and MNPs amounts are performed. The fully validated inhibition method is applied to real samples of spiked human serum from male AB plasma samples and pharmaceutical dosage forms containing MT. This novel MT detection method using an enzyme cascade blocking in a nanoparticle-based LOC and batch systems is also promising for other drugs that can inhibit Tyr or other enzymes.

Acknowledgement

We acknowledge MINECO (Spain) through Project MAT2011-25870. S. Kurbanoglu acknowledges the support given by Ankara University BAP14L0237002 for her Ph.D. thesis project.

Appendix A. Supplementary material

Supplementary data associated with this article can be found in the online version at http://dx.doi.org/10.1016/j.bios.2014.10.014.

References

Aslanoglu, M., Peker, N., 2003. J. Pharm. Biomed. Anal. 33, 1143–1147.
Betancor, L., Fuentes, M., Dellamora-Ortiz, G., Lopez-Gallego, F., Hidalgo, A., Alonso-Morales, N., Mateo, C., Guisan, J.M., Fernandez-Lafuente, R., 2005. J. Mol. Catal. B: Enzym. 32, 97–101.
Chung, W.G., Park, C.S., Roh, H.K., Lee, W.K., Cha, Y.N., 2000. Jpn. J. Pharmacol. 84, 213–220.
DeWasch, K., De Brabander, H.F., Impens, S., Vandewiele, M., Courtheyn, D., 2001. J. Chromatogr. A 912, 311–317.
Duffy, D.C., McDonald, J.C., Schueller, O.J.A., Whitesides, G.M., 1998. Anal. Chem. 70, 4974–4984.
Economou, A., Tzanavaras, P.D., Notou, M., Themelis, D.G., 2004. Anal. Chim. Acta 505, 129–133.
Edward, A.C., 1992. In: Smith, C.M., Reynard, A.M. (Eds.), Textbook of Pharmacology. Saunders, Philadelphia, pp. 652–656.
Ermer, J.M., 2005. JHMcB Method Validation in Pharmaceutical Analysis. Weinheim, Wiley: VCH.
Gheibi, N., Saboury, A.A., Mansuri-Torshizi, H., Haghbeen, K., Moosavi-Movahedi, A. A., 2005. J. Enzyme Inhib. Med. Chem. 20, 393–399.
Grieshaber, D., MacKenzie, R., Vörös, J., Reimhult, E., 2008. Sensors 8, 1400–1458.
Hashizume, Y., Yamaki, T., Hidaka, H., 1977. Br. J. Pharm. 59, 157–162.
Hollosi, L., Kettrup, A., Schramm, K.W.M., 2004. J. Pharm. Biomed. 36, 921–924.
Kasraee, B., 2002. J. Investig. Dermatol. 118, 205–207.
Kortmann, H., Blank, L.M., Schmid, A., 2009. Lab Chip 9, 1455–1460.
Kuwabara, T., Tomita, E., Sakita, S., Hasegawa, D., Sone, K., Yagi, M., 2008. J. Phys. Chem. C 112, 3774–3779.
Lerch, K., 1981. Copper monooxygenases: tyrosinase and dopamine lhydroxylase, in: Metal Ions in Biological Systems. Marcel Dekker, New York.
Li, K., Lai, Y., Zhang, W., Jin, L., 2011. Talanta 84, 607–613.
Li, X., Zhang, F., Shi, J., Wang, L., Tian, J.H., Zhou, X.T., Jiang, L.M., Liu, L., Zhao, Z.J., He, P.G., Chen, Y., 2011. Electrophoresis 32, 3201–3206.
Marn, S., Merkoçi, A., 2012. Electroanalysis 24, 459–469.
Mason, H.S., 1957. Mechanisms of oxygen metabolism.. In: Nord, F.F. (Ed.), Advan. Enzymol.. Academic Press, NewYork, pp. 79–234.
Mayorga-Martinez, C.C., Cadevall, M., Guix, M., Ros, J., Merkoçi., A., 2013a. Biosens. Bioelectron. 40, 57–62.
Mayorga-Martinez, C.C., Hlavata, L., Miserere, S., López-Marzo, A., Labuda, J., Pons, J., Merkoçi, A., 2013b. Electrophoresis 34, 2011–2016.
Mayorga-Martinez, C.C., Hlavata, L., Miserere, S., López-Marzo, A., Labuda, J., Pons, J., Merkoçi, A., 2014a. Biosens. Bioelectron. 55, 355–359.
Mayorga-Martinez, C.C., Madrid, R.E., Felice, C.J., 2008. Sensor. Actuators B-Chem. 133, 682–686.
Mayorga-Martinez, C.C., Pino, F., Kurbanoglu, S., Rivas, L., Ozkan, S.A., Merkoçi, A., 2014b. J. Mater. Chem. B 2, 2233–2239.
Medina-Sánchez, M., Miserere, S., Marín, S., Aragay, G., Merkoci, A., 2012a. Lab Chip 12, 2000–2005.
Medina-Sánchez, M., Miserere, S., Merkoci, A., 2012b. Lab Chip 12, 1932–1943.
Ozkan, S.A., 2012. Electroanalytical Methods in Pharmaceutical Analysis and Their Validation. HNB Publishing, New York.
Papouchado, L., Petrie, G., Sharp, J.H., Adams, R.N., 1968. J. Am. Chem. Soc. 90, 5620–5621.
Papouchado, L., Petrie, G., Sharp, J.H., Adams, R.N., 1972. J. Electroanal. Chem. 38, 389–395.
Pérez-López, B., Merkoçi, A., 2011. Adv. Funct. Mater. 21, 255–260.
Pumera, M., Merkoçi, A., Alegret, S., 2006. Trends Anal. Chem. 25, 219–235.
Raoofz, J.B., Ojani, R., Amiri-Aref, M., Chekin, F., 2012. Russ. J. Electrochem. 48, 450–456.
Rayn, M.D., Yueh, A., Wen-Yu, C., 1980. J. Electrochem. Soc. 127, 1489–1495.
Ren, K., Zhou, J., Wu, H., 2013. Acc. Chem. Res. 46, 2396–2406.
Ren, K., Zhou, J., Wu, H., 2014. Curr. Opin. Biotechnol. 25, 78–85.
Renaudot, R., Agache, V., Fouillet, Y., Laffite, G., Bisceglia, E., Jalabert, L., Kumemur, M., Collar, D., Fujitac, H., 2013. Lab Chip 13, 4517–4524.
Siénko, D., Gugała, D., Nieszporek, J., Jankowska, J., Saba, 2006. J. Electrochim. Acta 51, 2273–2277.
Solomon, E.I., Sundaram, U.M., Machonkin, T.E., 1996. Chem. Rev. 96, 2563–2606.
Stonea, C.G., Cardosib, M.F., Davis, J., 2003. Anal. Chim. Acta 491, 203–210.
Tang, L., Lee, N.Y., 2010. Lab Chip 10, 1274–1280.
Tolosa, V.M., Wassumb, K.M., Maidment, N.T., Monbouquette, H.G., 2013. Biosens. Bioelectron. 42, 256–260.
Xia, Y., Whitesides, G.M., 1998. Annu. Rev. Mater. Sci. 28, 153–184.
Yazhen, W., 2011. Bioelectrochemistry 81, 86–90.
Yeh, C.H., Chang, Y.H., Chang, T.C., Lin, H.P., Lin, Y.C., 2010. Analyst 135, 2717–2722.
Zhang, L., Liu, Y., Xie, M.X., Qiu, Y.M., 2005. J. Chromatogr. A 1074, 1–7.